Water Resources Research®

Key Points:

- (Sub-) Pore-scale microplastics were advectively transferred from the surface water into the streambed sediments in flume experiments
- Infiltration patterns depend on microplastic size, streambed sediment type and surface flow velocities
- Microplastic retention was observed for 10 µm beads, 1 µm beads were considerably retarded in fine sediments

Correspondence to:
J.-P. Boos,
Jan-Pascal.Boos@uni-bayreuth.de

Assessing the Behavior of Microplastics in Fluvial Systems: Infiltration and Retention Dynamics in Streambed Sediments

Jan-Pascal Boos[1] , Franz Dichgans[2] , Jan H. Fleckenstein[2,3] , Benjamin Silas Gilfedder[1,4] , and Sven Frei[5]

[1]Department of Hydrology, Bayreuth Center of Ecology and Environmental Research (BAYCEER), University of Bayreuth, Bayreuth, Germany, [2]Department of Hydrogeology, UFZ – Helmholtz Centre for Environmental Research, Leipzig, Germany, [3]Hydrologic Modeling Unit, Bayreuth Center of Ecology and Environmental Research (BAYCEER), University of Bayreuth, Bayreuth, Germany, [4]Limnological Research Station, Bayreuth Center of Ecology and Environmental Research (BAYCEER), University of Bayreuth, Bayreuth, Germany, [5]Wageningen University Research Centre, Department of Environmental Science, Aquatic Ecology and Water Quality Management Group, Wageningen, The Netherlands

Abstract Microplastics (MPs) have been detected ubiquitously in fluvial systems and advective transfer has been proposed as a potential mechanism for the transport of (sub-) pore-scale MPs from surface waters into streambed sediments. However, the influence of particle and sediment properties, as well as the hydrodynamic flow regime, on the infiltration behavior and mobility of MPs in streambed sediments remains unclear. In this study, we conducted a series of flume experiments to investigate the effect of particle size (1–10 µm), sediment type (fine and coarse sand), and flow regime (high/low flow) on particle infiltration dynamics in a rippled streambed. Quantification of particles in the flume compartments (surface flow, streambed interface, and in the streambed) was achieved using continuous fluorescence techniques. Results indicated that the maximum infiltration depth into the streambed decreased with increasing particle size (11, 10, and 7 cm for 1, 3, and 10 µm). The highest particle retardation was observed in the fine sediment experiment, where 22% of the particles were still in the streambed at the end of the experiment. Particle residence times were shortest under high flow conditions, suggesting that periods of increased discharge can effectively flush MPs from streambed sediments. This study provides novel insights into the complex dynamics of MP infiltration and retention in streambed sediments and contributes to a better understanding of MPs fate in fluvial ecosystems. Quantitative data from this study can improve existing modeling frameworks for MPs transport and assist in assessing the exposure risk of MPs ingestion by benthic organisms.

Plain Language Summary Microplastics (MPs) (small plastic particles) are present in river systems worldwide. The processes that lead to their transport and retention in rivers are not fully understood. Scientists have proposed that the infiltration of surface water into the streambed can carry MPs with it. In this study, we conducted experiments in a controlled environment that resembles a stream and its streambed. We investigated how different sizes of plastic particles (1, 3, and 10 µm), the types of sediment (fine and coarse sand), and water flow rates (low and high) affect how far particles travel in a streambed. We found that the size of MPs played a significant role in their depth of infiltration. Larger particles did not infiltrate as deeply as smaller particles, and were also retained in the streambed. Fine sand trapped particles for a longer time than coarse sand, and 22% of the particles remained in the streambed until the end of the experiment. Faster flowing water quickly removed MPs from the streambed. Our research helps understand how MPs spread in river systems and how long they remain in the streambed. The data can be used to improve transport models and assess the risk MPs pose to aquatic organisms.

1. Introduction

Plastic production has continuously increased over the last decades (PlasticsEurope, 2022). After usage, the majority of plastic waste is not properly managed (Lebreton & Andrady, 2019) and plastic pollution in the environment is now a global concern (Persson et al., 2022). Microplastics (MPs), small polymer compounds smaller than 5 mm (Frias & Nash, 2019) have been ubiquitously detected in marine (Gola et al., 2021), limnic (Yang et al., 2022) and riverine environments (Eerkes-Medrano et al., 2015). MPs can be incorporated by aquatic biota (Scherer et al., 2018) and trigger adverse effects on the organism (Brehm et al., 2022). Following bioaccumulation in higher trophic levels (Bhatt & Chauhan, 2023), MPs are reported to threaten aquatic ecosystems

(Anbumani & Kakkar, 2018), which makes it crucial to understand the transport mechanisms governing the fate of MPs in fluvial systems (Horton & Dixon, 2018).

Traditionally, rivers and streams were treated as pure transport vectors, where MPs are transported to the oceans and eventually buried in deep sea sediments (Kumar, Sharma, Manna, & Jain, 2021; Meijer et al., 2021; Woodall et al., 2014). In recent literature, fluvial systems are also discussed as potential accumulation areas for MPs (van Emmerik et al., 2022), which can be retained by instream vegetation (Shi et al., 2022), on floodplains (Rolf et al., 2022), river banks (Liong et al., 2021) and in streambed sediments (Frei et al., 2019; Yang et al., 2021). MPs in rivers and streams are subject to a variety of transport processes (Kumar, Sharma, Verma et al., 2021) and exhibit unique transport characteristics (Waldschläger & Schüttrumpf, 2019) and transport modes compared to natural particles such as mineral sediments (Valero et al., 2022). Flow conditions (Haberstroh et al., 2020), channel characteristics (Mostefaoui et al., 2022) and particle properties (Ahmadi et al., 2022; Elagami et al., 2022) are the major controls for the hydrodynamic transport behavior of MPs in fluvial systems. Surface flow velocity has a direct effect on the abundance of MPs in streambed sediments (Eibes & Gabel, 2022): Low flow velocities, such as found in pool structures or near river banks, facilitate gravitational settling, and can lead to a temporal accumulation of MPs in streambed sediments (Hübner et al., 2020) which can be reversed during flooding (Ockelford et al., 2020).

The mechanisms controlling the transfer of MPs between the surface flow domain and the streambed sediments, as well as the factors influencing their mobility within porous media, remain only poorly understood. Similar to solutes, the transport of (sub-) pore-scale MPs into streambed sediments can be driven by hyporheic exchange (Boos et al., 2021; Frei et al., 2019). Instead of being transported conservatively through bedform structures and being released back into the stream (Brunke, 1999), MPs were found to infiltrate into shallow layers of the hyporheic zone, where they can be temporally or permanently immobilized (Harvey et al., 2012). Simulations from headwater streams suggest that characteristic MPs residence times within streambed sediments can vary across different temporal scales, ranging from a few hours to several years (Drummond et al., 2022). Lower density MPs exhibited highest mobility within streambed sediments (He et al., 2021). In column experiments, retention of MPs was found to be strongly affected by sediment properties such as type and content of clay minerals (Lu, Gilfedder, Peng, Niu, & Frei, 2021), the presence of iron-oxides as well as pore water chemistry (Lu, Gilfedder, Peng, Peiffer et al., 2021). Retention mechanisms in porous media are primarily dependent on particle size, where larger particles (>30 μm) are prone to mechanical straining within the pore space and where the mobility of smaller particles (≈1 μm) is affected by heteroaggregation with sediments (Herzig et al., 1970). In the range of 3–30 μm, particles exhibit a high mobility within the porous media due to little mechanical straining and aggregation. For larger MPs (>100 μm) column experiments have shown that the infiltration depth into coarse sediments primarily depends on the particle/sediment grain size ratio $D = d_{MP} d_{Sediment}^{-1}$ (Waldschläger & Schüttrumpf, 2020). To deepen our understanding of the transport behavior of MPs in streambed sediments further research beyond the limitations of simplified one-dimensional column experiments is necessary. It is necessary to consider more realistic hydrodynamic conditions as well as different MPs properties (e.g., size, density, shape and surface properties) and sediment characteristics (e.g., grain size distribution, permeability and mineral composition) (Waldschläger et al., 2022).

Recently, a quantitative method was developed for the spatiotemporal analysis of transport mechanisms of MPs in an experimental flume environment (Boos et al., 2021). Experiments have shown that (sub-) pore scale MPs are advectively transferred into streambed sediments through infiltrating stream water along defined flow paths, supporting the hypothesis that hyporheic exchange is a significant mechanism for the transfer of small MPs into streambed sediments (Boos et al., 2021). In these experiments, propagation of 1 μm polystyrene beads through the streambed resembled a pattern commonly encountered for solutes (Elliott & Brooks, 1997; Thibodeaux & Boyle, 1987): Particles infiltrated at the upstream stoss side of ripple structures, propagated through the sediment following the hydraulic head gradient and were released at the downstream lee side. Although the experimental setup was limited to a specific combination of MPs (1 μm polystyrene beads), sediment types (mean diameter 1 mm) and hydrodynamic forcing (mean velocity 0.17 m s⁻¹) important insights into the complex behavior of MPs in fluvial systems were gained.

Building on previous work by Boos et al. (2021), we utilized quantitative methods to further explore the transport behavior of MPs in the surface water, at the streambed interface and within streambed sediments. The objective of this study is to investigate the influence of particle size (1–10 μm) on the infiltration dynamics and
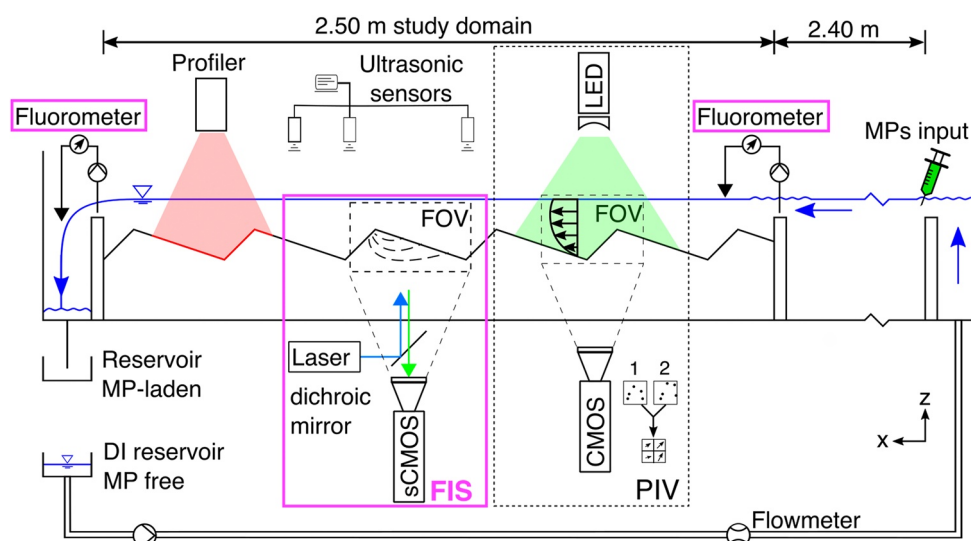
Figure 1. Schematics of the experimental flume setup: Tracking of Microplastics in the surface water (fluorometers) and within the streambed sediments Fluorescence-Imaging-System (FIS), and hydrodynamic measurements with Particle-Image-Velocimetry (PIV), complemented by water level measurements with ultrasonic sensors and bedform elevation measurement with a laser profiler. Note that FIS and PIV were consecutively applied at the same bedform. Modified after Boos et al. (2021).

penetration depths of MPs in different streambed sediments (fine/coarse sand) under varying hydrodynamic conditions (low/high flow). For this purpose, we performed a set of experiments using fluorescent MPs in an experimental flume environment in combination with sediments to represent typical rippled bedform structures found in fluvial systems. The experiments provided quantitative data that was used to estimate particle retardation capacities in streambed sediments as well as spatially distributed information about the particle mobility in rippled bedform structures. Computational Fluid Dynamics (CFD) simulations were used for the characterization of the hydrodynamic forcing at the streambed interface that controls hyporheic exchange and to better understand the flow conditions in the streambed sediments.

2. Materials and Methods

2.1. Flume Setup and Hydrodynamic Measurements

Transport experiments were carried out in an open-circuit flume (5 • 0.086 • 0.30 m, HM 160, G.U.N.T. GmbH), with an elevation gradient of 3 mm/m (Figure 1). The discharge in the flume (1–2 m^3 hr^{-1}) was continuously monitored using an electromagnetic flowmeter (flowTRANS MAG S01, Jumo GmbH) and resulted in surface flow velocities of approximately 0.07–0.11 m s^{-1}. The flume was operated using deionized water to avoid MPs aggregation. Water temperature was monitored using a temperature logger (Model 3001, Solinst Canada Ltd). A study domain within the flume was defined using a weir plate at $x = 2.40$ m distance from the flume inlet and a V-notch weir at $x = 4.90$ m, both were 15 cm high. An additional weir plate was positioned at the inlet ($x = 0$ m) to provide a homogeneous inflow.

Within the study domain, the streambed was manually formed from unimodal sands of two different types for the different experiments, characterized by a mean diameter of 1.0 mm (coarse) and 0.4 mm (fine). The streambed consisted of a series of 9 consecutive ripple structures, closely resembling a geometry commonly found in natural streams (Haque & Mahmood, 1985), with a height of 2.8 cm and a length of 20 cm of which 58% corresponded to the stoss side. The bedform morphology was measured along a 50 cm transect (including multiple ripple structures) using a 2D laser profile sensor (MLSL226, wenglor sensoric GmbH), which allowed us to monitor bedform stability during the experiments (Figure S1 in Supporting Information S1). After the experiment, the entire streambed elevation profile in the flume was measured using the laser profiler (measurement resolution of 4 mm^{-1}).

The water surface elevation was measured using 6 ultrasonic sensors (UFP 200, WayCon GmbH), providing information on the local water surface slope and an estimate of the discharge from the weir head, using Thompson

Table 1
Characteristics of the Experiments.

ID [-]	d_{MP} [µm]	d_S [µm]	$D = d_{MP}$ d_S^{-1} [1]	Q [m³h⁻¹]	$\bar{v}_x$ [ms⁻¹]	m_0 [mg]
1 µm	1	1032	0.0010	1.09	0.076	54
3 µm	3	1032	0.0029	1.09	0.070	98
10 µm	10	1032	0.0097	1.00	0.079	78
Fine sand	1	357	0.0028	1.05	0.066	53
High flow	1	1032	0.0010	2.15	0.114	28

Note. d_{MP} refers to the microplastic (MP) diameter, d_S to the mean sediment diameter, $D = d_{MP} d_S^{-1}$ the particle/sediment grain size ratio, Q is the discharge, $\bar{v}_x$ is the mean longitudinal velocity in the surface flow (calculated from Particle-Image-Velocimetry measurements) and m_0 is the total input mass of MPs.

overflow coefficients. The 2D surface flow velocities along the longitudinal and vertical axis (x-z-plane) were measured using Particle-Image-Velocimetry (PIV). An LED sheet ($\lambda \approx 520$ nm, LPS3, iLA_5150 GmbH) illuminated a flow section along the flume centerline and images were acquired with a CMOS camera (UI3370, iDS Imaging GmbH), mounted on an optical rail. The flow field was measured over a selected bedform, between $x = 3.65$ m and $x = 3.85$ m, as well as its two adjacent ripples. 9 individual PIV measurements were merged, each using time averages of 1000 frames acquired at 40 Hz with a spatial resolution of 136 µm/pixel.

2.2. Experimental Procedure

Five different experiments were carried out to investigate the influence of (a) particle sizes (1, 3 and 10 µm beads), (b) sediment types (fine and coarse sand), and (c) hydrodynamic flow conditions (low/high flow) on the particle infiltration patterns and dynamics (characteristics of the experiments are provided in Table 1). The experiment using 1 µm particles, low flow conditions and coarse sediment was used as a reference case. Prior to all experiments, the measurement systems were calibrated, and the flume including the sediments were cleaned with deionized water to remove any residual MPs from previous work. A rippled streambed was formed and before the experiments started, the flume was run in a closed circuit for 2 h, and until optical inspection assured bedform stability. For the experiments, the water circuit was opened, and a concentrated MPs suspension was injected as a pulse into the surface flow at the inlet of the flume. Experiments were terminated after 30 min, after which concentrations in the outflow were below the detection limit, and optical inspection suggested no major change in MPs abundances in the monitored bedform. The input mass of MPs was chosen based on the particle size, flume discharge, and logistical constraints, to achieve ideal conditions to record the concentrations in the experiments. Importantly, the differences in initial masses are highly unlikely to significantly impact transport processes in both the surface water and the streambed. This is due to the fact that (a) the MPs were coated with a surfactant to prevent homoaggregation and (b) the overall mass of applied MPs (approximately 50 mg) is orders of magnitude lower than the sediment mass within the flume (approximately 50 kg), effectively ruling out any substantial streambed clogging processes.

2.3. Microplastic Detection and Quantification

The experiments were carried out with polystyrene microbeads with diameters of 1, 3 and 10 µm and a density of 1050 kg m⁻³ (Fluoresbrite® Plain YG Microspheres, PolySciences Inc.). The particles were internally coated with a fluorophore characterized by a maximum excitation and emission wavelength of 441 and 486 nm, respectively. Details about the coating process are considered confidential by the manufacturer. MPs monitoring is based on novel fluorometric techniques presented in Boos et al. (2021): Continuous detection of MPs-concentrations in the in- and outflow of the study domain of the flume was achieved by using portable fluorometers (GGUN FL-24, Albillia Co.) which were positioned at the weir overflows at $x = 2.40$ m and $x = 4.90$ m, measuring at 0.5 Hz (Figure 1). At the bedform structure selected for detailed study, between $x = 3.65$ m and $x = 3.85$ m, a Fluorescence-Imaging-System (FIS) was used to analyze MPs transport in the surface flow, at the streambed interface and in the streambed sediments near the glass interface of the flume. Two continuous-wave diode-pumped solid-state lasers (MBL-F-457, CNI Ltd) were used to excite the fluorescent particles and a scientific complementary metal-oxide-semiconductor (sCMOS) camera (Andor Zyla 5.5, Oxford Instruments) captured fluorescence images with a spatial resolution of 170 µm/pixel, using an exposure time of 100 ms and a frame rate of 8 Hz.

The MPs mass concentrations at the in- and outflow location of the surface water were normalized according to Equation 1 to allow for a comparison between the individual experiments. A normalized mass transfer (NMT) $\dot{m}$ [T⁻¹] was calculated using c [ML⁻³] the measured particle concentration, Q [L³T⁻¹] the observed discharge in the flume and m_0 [M] the mass of MPs input.

$$\dot{m}_{in,out}(t) = \frac{c_{in,out}(t) \cdot Q(t)}{m_0} \tag{1}$$

For any time t, integration of the NMT yields the total mass of MPs that has entered respectively left the study domain. The difference between the in- and outflow mass was normalized by the inflow mass, and this mass fraction was interpreted as MPs present in the study domain. At the end of each experiment the integration of the NMT at the in- and outlet yields a MPs recovery rate that was used to compare MPs retention for the different experimental scenarios.

MPs abundances in the control bedform were continuously quantified using the method outlined in Boos et al. (2021), where abundances were estimated by systematically analyzing the spatially averaged light intensities of the FIS images (Text S1 in Supporting Information S1). Detection limits for MPs in the streambed sediments were estimated from the calibration curve (Funk et al., 1985) and normalized using Equation 1. Spatial infiltration dynamics of MPs into the monitored bedform were estimated by extracting breakthrough curves at different depths (1–11 cm) below the ripple crest from the FIS monitoring (averaging depth for each breakthrough curve was 1 cm). Depth-specific breakthroughs were additionally filtered by rejecting the earliest and latest 5% of MPs detection in order to exclude outliers and reduce experimental artifacts. The start of MPs detection in each layer represented the arrival of the plume front and from the slope $\partial z/\partial t$, depth-specific vertical propagation velocities were calculated.

Due to the limited resolution of the FIS, it was not possible to track individual 1 and 3 μm particles within the monitored streambed. Resolution was however sufficient for the larger 10 μm particles, allowing to monitor their positions in a 2D plane of the bedform by using "blob" detection algorithms (The MathWorks Inc, 2019). Here, a pre-defined mask was used to differentiate between particles that infiltrated at the stoss side and particles which deposited from the surface water on the lee side of the bedform. Only images with more than 20 detected particles were used in the analysis. Infiltration dynamics was assessed using two aggregated metrics: (a) The center of mass of the particle cloud was calculated by averaging the individual positions and (b) the front of the infiltration plume was obtained by connecting the outermost particles.

2.4. Integrated Simulation of Surface and Porous Media Flow

To gather additional insight on the hydraulic conditions in the flume, a numerical model was built using the computational fluid dynamics toolbox OpenFOAM. The 3D integral model of surface and subsurface flow was solved using the multiphase solver interFoam. To accurately resolve the turbulent flow, specifically on the lee side of each ripple, turbulence was modeled using Large-Eddy-Simulation algorithms. The numerical model was built as direct representation of the geometries of the flume and the bedforms and used the measured information on hydrodynamical characteristics of the flow for model calibration. Additional details about the numerical model are given in Text S2 in Supporting Information S1. The methodology is also described and validated in Dichgans et al. (2023). By employing the integrated hydro-numerical model, the data set gained through the laboratory equipment can be augmented specifically in regard of the subsurface flow field and the hydrodynamic forcing at the streambed interface, which cannot be captured accurately through a physical recording in the laboratory.

3. Results

3.1. Hydrodynamic Characterization of the Flow

In the surface water compartment, the flow regime is separated into a fast-flowing upper region and a slower bottom-near region (Figures 2a–2d). This flow separation was observed for both low flow, and high flow regimes. For the low flow experiments, the mean horizontal velocity was $\bar{v}_{x,\text{top}} = 0.11$ m s^{-1} in the upper flow regime and $\bar{v}_{x,\text{bottom}} = 0.03$ m s^{-1} in the lower regime. Figures 2e and 2f show the 2D distribution of vertical velocity components in the surface water above the monitored bedform within the study domain of the flume. In all experiments, low-velocity recirculation eddies developed in the valley areas of the bedforms with flow components directed downwards for the stoss sides and upwards for the lee sides (Figures 2e and 2f).
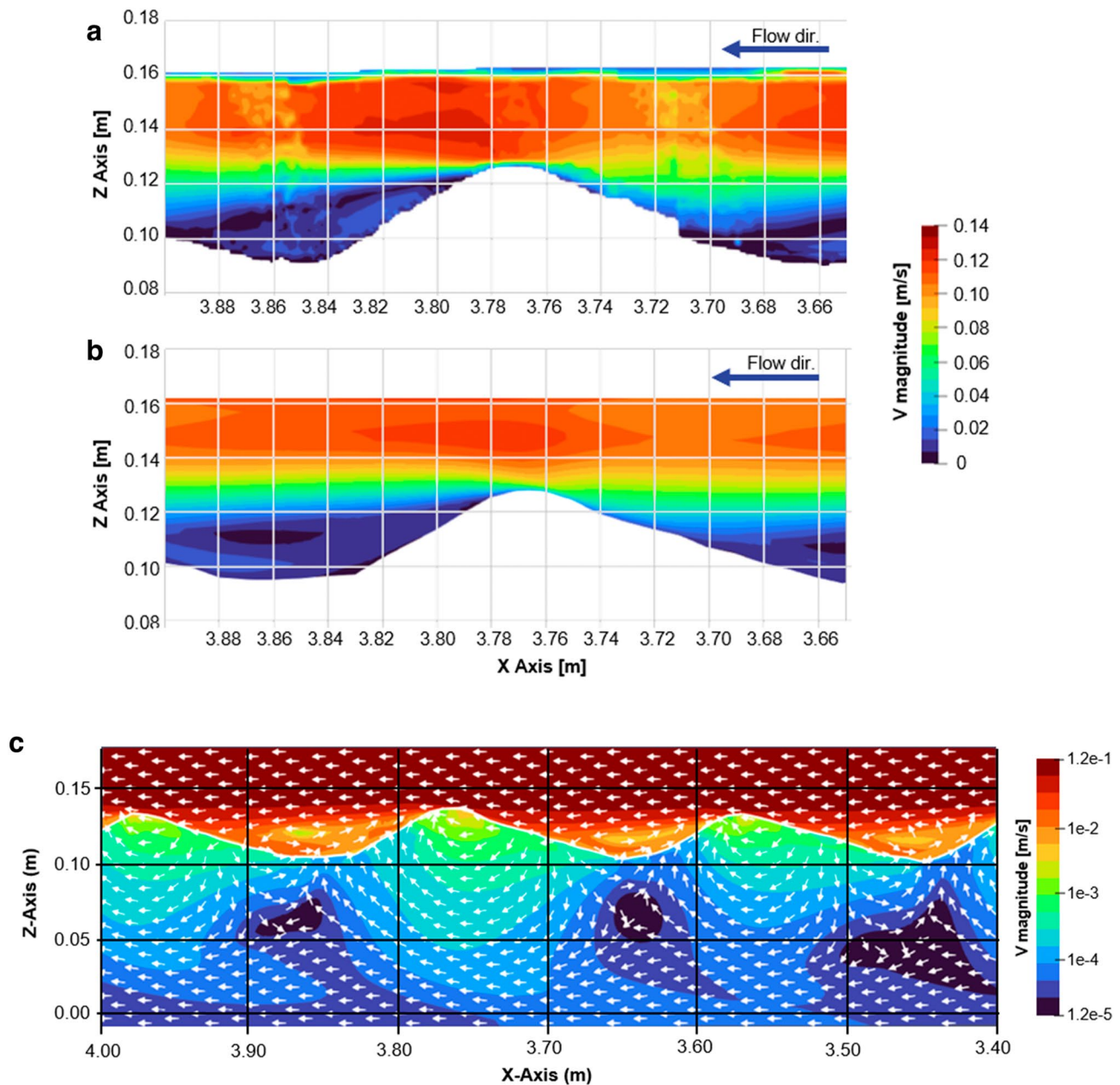
The numerical model reproduced the surface flow field accurately (Figures 3a and 3b). Minor differences were observed in direct proximity to the overflow section of the ripple crest (0.01–0.02 m s^{-1}). This deviation was acceptable, given the turbulent flow conditions in the surface water, and a non-uniform flow field that varied over
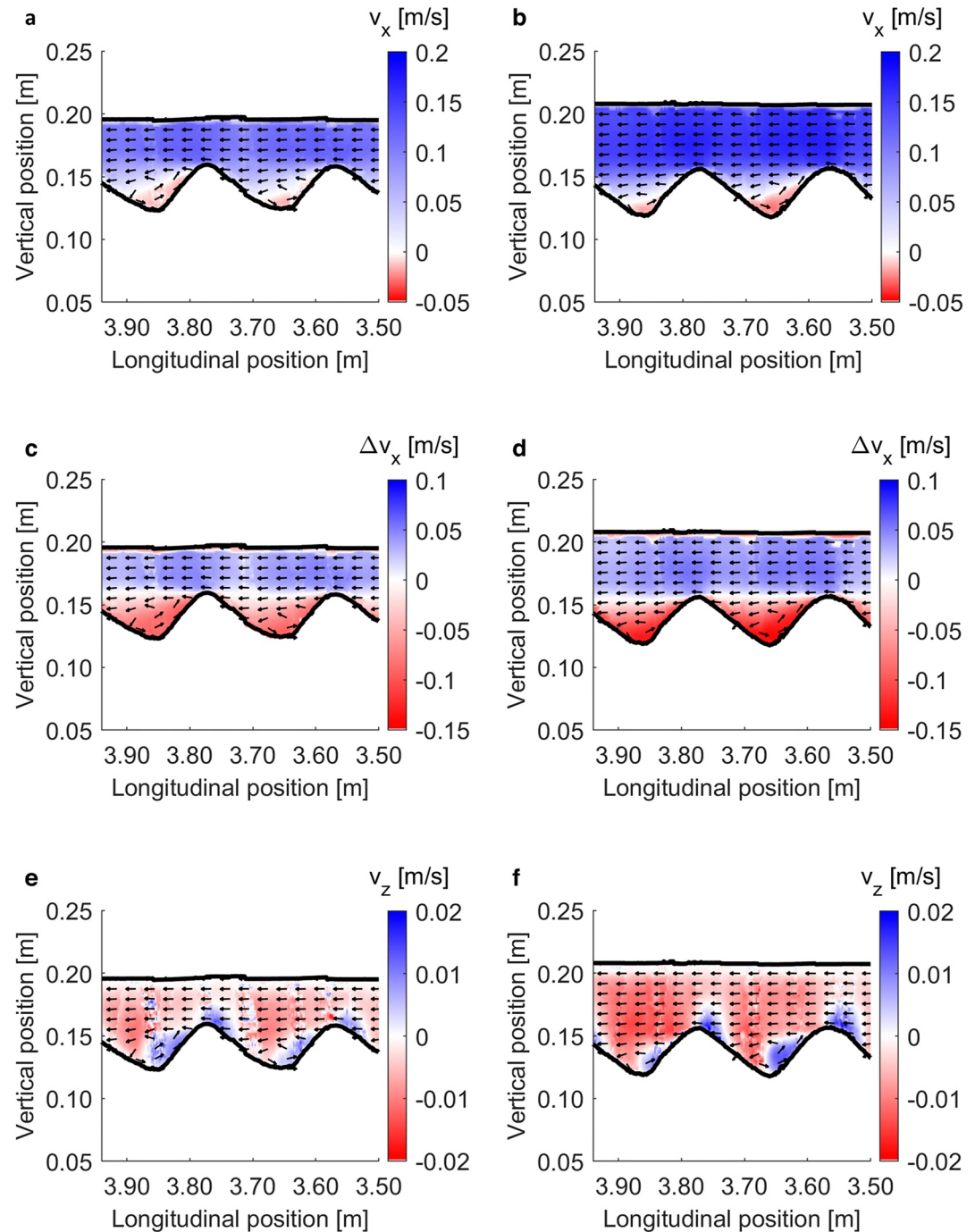
Figure 2. Hydrodynamic characterization of the surface flow field at the monitored bedform. First column (a,c,e): low-flow (reference) experiment, second column (b,d,f): high-flow experiment. (a) and (b): Horizontal velocity components, mean flow direction was from right to left. (c) and (d): Difference between local velocity and mean velocity in longitudinal direction, indicating a separation into a rapidly flowing upper region and a low-flow area in proximity to the ripples. (e) and (f): Vertical velocity components, red colors indicate downward flow, blue colors upward flow.

the flume width. Within the subsurface, individual flow cells developed under the ripples (Figure 3c). Beneath the flow cells, a continuous underflow layer was forming. Hyporheic flow depended on surface flow, and water entered at the upstream stoss side, and left at the downstream lee side, in proximity to the ripple crest. Subsurface flow velocities ranged between 0.01–2 mm s^{-1}.

Figure 3. Velocity magnitudes in the low-flow (reference) experiment. Results for the surface flow obtained from (a) Particle-Image-Velocimetry, and (b) the openFOAM model show a close correlation. The numerical model additionally yields information on the subsurface flow domain (c).

3.2. Quantification of Particle Breakthrough and Retention

Figure 4a shows the NMT breakthrough curves for the different experiments which were measured in the surface water, using the fluorometer installed at the outflow location of the study domain. Initial timing of the particle breakthrough was similar for all experiments using low flow conditions and coarse sediments (Figure 4a). Here peak arrival times at the outflow were almost identical for the 1, 3 and 10 μm particles (136–146 s). In comparison to the reference experiment with 1 μm particles, peak NMT was higher for both 3 μm particles (+17%) and 10 μm particles (+9%). In the experiment with fine sediments, migration of the particle plume in the study domain was slowest as indicated by the longer peak arrival time of 168 s and peak mass 14% lower than the reference. In the high flow experiment, peak NMT was 77% higher than in the reference experiment and the peak was observed after 89 s, which was the fastest peak arrival time among all experiments.
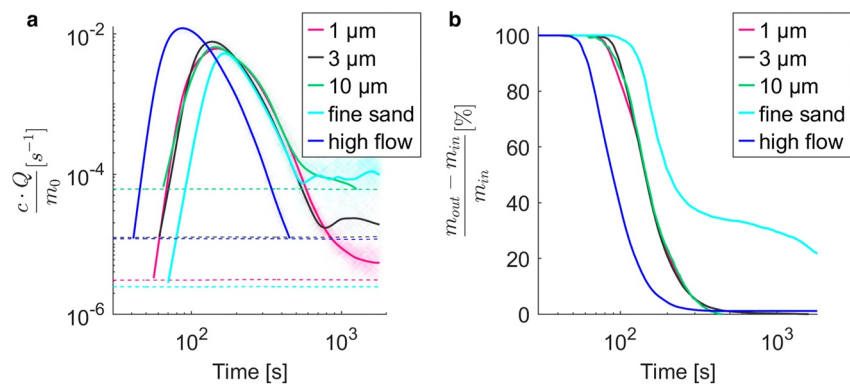
Figure 4. Results of surface water concentration measurements. (a) Normalized microplastics (MPs) mass transfer rates for the experiments measured at the outflow location of the study domain. Dashed lines indicate size-dependent, individual quantification limits, obtained from the calibration procedure, and normalized with Equation 1. (b) Temporal evolution of MPs mass stored in the study domain for the different experiments. The 1 μm run was the reference experiment.

NMTs for the 3 and 10 μm particles decreased more slowly during the receding limb of the breakthrough curves compared to the 1 μm particles, indicating a higher particle residence time in the study domain (Figure 4a). Higher residence times for the 3 μm particles are further supported by the presence of a secondary peak in the tail of the breakthrough curve. This secondary peak indicates a late increase in particle concentration in surface flow and we attributed this to the release of particles from the streambed sediments. Multiple secondary peaks can also be observed in the tail of the breakthrough curve for the experiment with fine sediments (Figure 4a). This experiment shows the highest particle concentrations in surface flow at the end of the experiment, indicating high particle residence times in the study domain. Particle concentrations for the high flow experiment fell below the detection limit after 450 s, which precluded any meaningful characterization of the tailing behavior and dynamics of particle retention.

MPs storage in the study domain was comparable for the different MPs sizes and was <5% after 304–307 s (Figure 4b). Stored mass fractions showed the most rapid decrease in the high flow experiment, with 95% of the total particle mass being flushed out from the study domain after 191 s. For the fine sediment experiment, 60% of the total mass was rapidly flushed (within 266 s) from the study domain through the surface flow. Afterward, MPs was slowly released over time, suggesting particle release from the streambed sediments. At the end of the fine sediment experiment, a significant mass of particles (22%) was still present in the study domain.

3.3. Particle Infiltration Dynamics and Penetration Depths

For all experiments the central bedform in the study domain was continuously monitored using the FIS to both visualize and estimate particle concentrations in the streambed sediments. Figure 5 presents different frames of the FIS monitoring sequence (t = 300, 600, 1200, and 1800 s) containing the NMT. Movie S1 additionally shows the progress of the individual experiments. FIS monitoring indicated that particles entered the streambed at the upstream stoss side of a ripple and exited at the downstream lee side near the crest. This spatial infiltration pattern was consistent for the 1 and 3 μm particles. In contrast, the 10 μm particles only infiltrated into the most superficial layers of the sediment before becoming immobilized for the remaining duration of the experiment (Figures 5, 10 μm sequence). In the experiment using fine sediments, particles only infiltrated into the shallowest areas below the streambed interface at the stoss side of the ripple structure (Figure 5, fine sand sequence). Similar to the 10 μm experiment, a high fraction of particles that infiltrated into the fine sediments remained in the bedform, as indicated by frames taken at the end of the experiments, t = 1800 s. In the high flow experiment, particles were more efficiently flushed from the bedform structure as indicated by the low residual concentrations at the final monitoring FIS frame.

Detectable particle infiltration for the 1 μm particles (reference experiment) began at t = 154 s, and particles reached a maximum depth of 11 cm below the streambed interface after 1477 s (Figures 6a and 6b). The onset of detectable infiltration for the 3 μm particles was similar to the reference experiment (t = 152 s), but the maximum infiltration depth of 10 cm was slightly lower compared to the 1 μm particles. For the 10 μm particles detectable
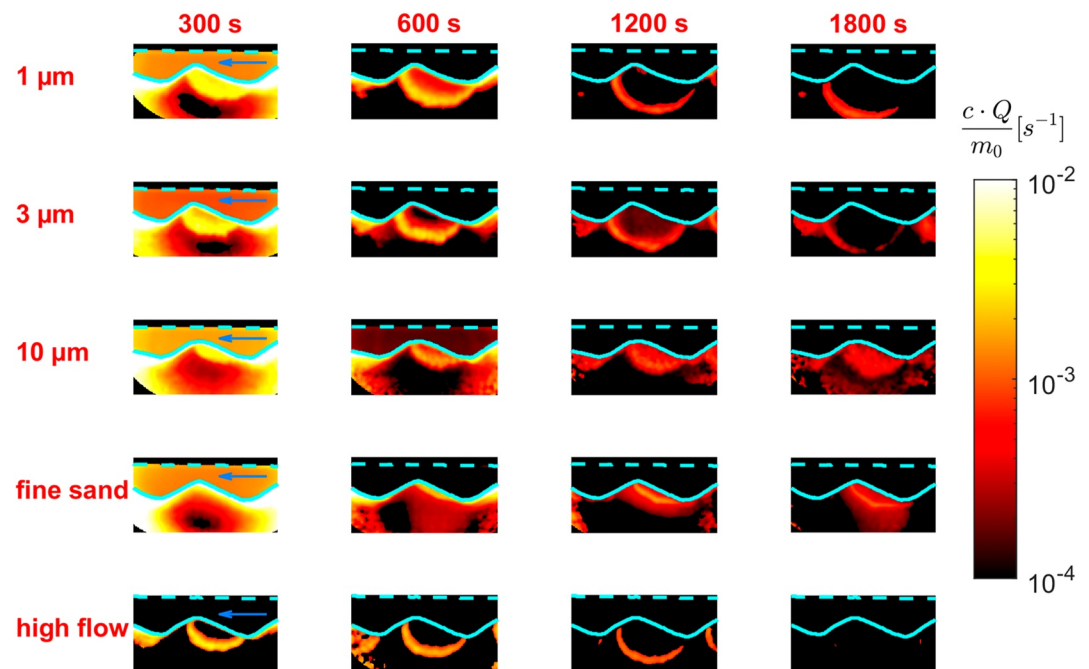
Figure 5. Planar normalized microplastic mass transfer rates for the 5 different experiments at 4 times, showing particle infiltration into the streambed sediments. The streambed interface is shown as solid line, the air-water-interface as dashed line, both in cyan color. The main direction of surface flow is from right to left, as indicated by a blue arrow at $t = 300$ s. Concentrations below the limits of quantification are discarded.

infiltration into the streambed occurred at $t = 449$ s, showing a high time delay (+294 s) compared to the reference experiment. Here particles only reached a maximum depth of 7 cm below the streambed interface. For the high flow experiment, the onset of detectable infiltration was the fastest among all experiments ($t = 121$ s), and particles reached a maximum depth of 10 cm after 1504 s. In the experiment using fine sediments, onset of particle infiltration was significantly delayed, occurring at $t = 547$ s and the maximum penetration depth of 5 cm was the lowest of all experiments. However, detection of MPs in the first 5 cm of the subsurface was nearly simultaneous for this experiment, and the data showed implausible gradients in layers deeper than 5 cm. All other experiments demonstrated consistent infiltration dynamics (Figures 6c and 6d), with high vertical propagation velocities occurring in the uppermost layers (~4 cm) below the ripple crest and an approximately exponentially decreasing trend in vertical propagation velocities with depth.

The resolution of the FIS camera was sufficient to track the fluorescent signal of individual particles through the bedform structure during the 10 μm experiment (Figure 7b). The peak of the particle count in the streambed was reached after 305 s where in total 937 particles were detected below the monitored bedform at the glass interface. During the experiment, the particle plume's center of mass moved along a trajectory approximately perpendicular to the stoss side of the ripple (Figure 7a). Propagation velocity for both, the center of mass and the plume front, initially was higher compared to later stages of the experiment, as indicated by the distance between consecutive crosses and solid lines in Figure 7a. After approximately 1500 s, both the center of mass and the plume front reached their final position, suggesting temporary or permanent immobilization of the 10 μm particles within the bedform (Figure S4 in Supporting Information S1). At the end of the experiment at $t = 1800$ s, still around 300 particles (Figure 7c) were located in the observable part of the bedform.

4. Discussion

Characterization of hydrodynamic flow conditions in the surface flow by combining PIV measurements and CFD modeling showed the presence of flow separation and the formation of recirculating eddies downstream of the rippled bedforms. The eddies and the streambed topography were responsible for an irregular distribution of dynamic and hydrostatic pressure heads over the streambed interface, driving hyporheic exchange. The hyporheic
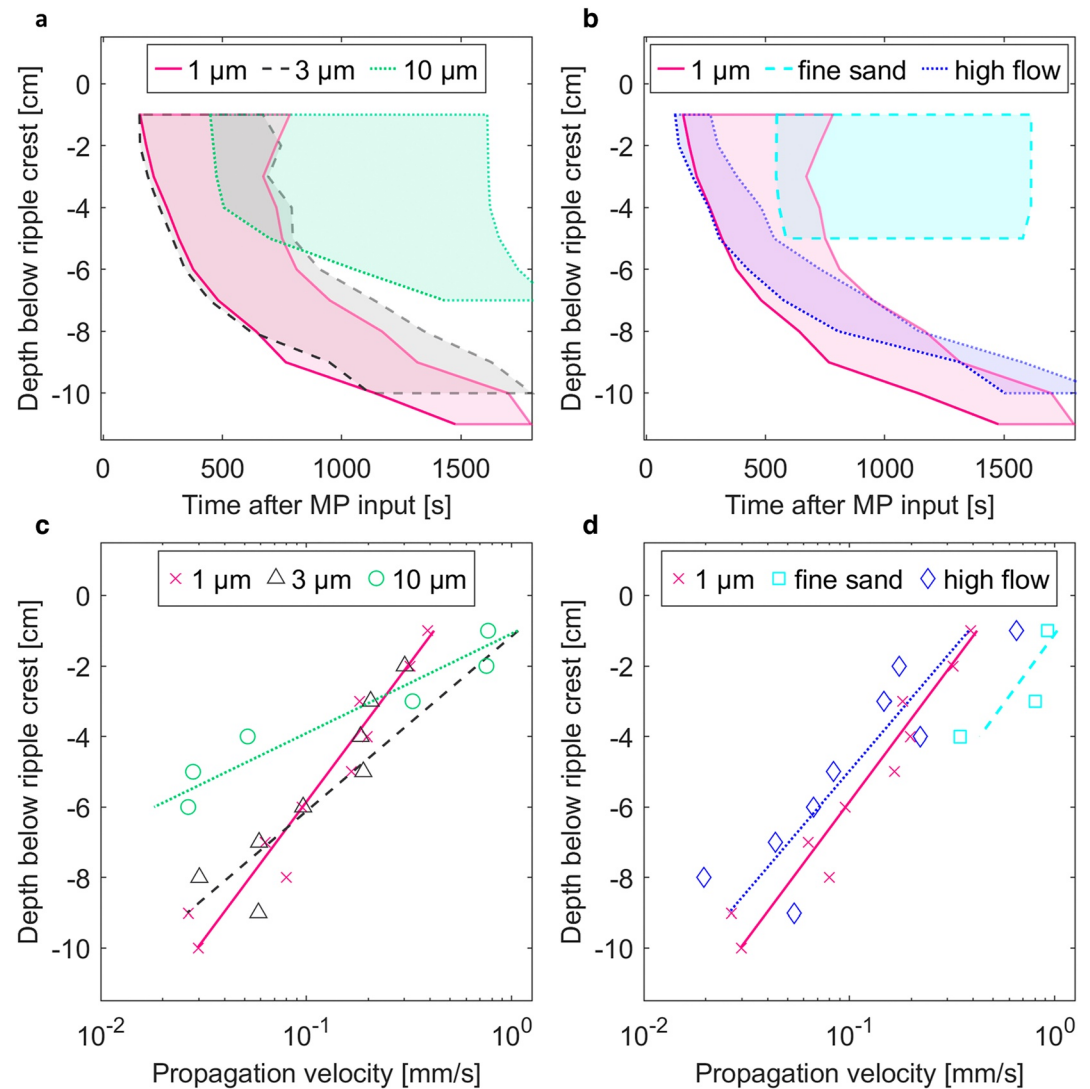
Figure 6. Particle infiltration dynamics below the ripple crest. (a–b): Infiltration depth as a function of time: Shaded areas correspond to the areas of variation based on the 5%–95% particle breakthrough criterium, highlighting the arrival of the plume front. (c–d): Vertical propagation velocities, calculated from the plume front arrival times, fitted to an exponential trendline.

flow field exhibited spatial patterns that are commonly described in literature for bedform-induced hyporheic exchange, where infiltration occurs at the stoss side and exfiltration at the lee side of the bedform structure (e.g., Elliott and Brooks (1997); Frei et al. (2018); Janssen et al. (2012); Trauth et al. (2014)). The FIS monitoring demonstrated that MPs between 1 and 10 μm were advectively transferred across the streambed interface with the preferential infiltration location at the stoss side of the bedform. While pore-scale MPs (<100 μm) have been found in high abundances in streambed sediments (Frei et al., 2019; Hurley et al., 2018), particles in this size class do not settle easily under the turbulent flow regimes found in rivers and streams. Our findings provide clear evidence that hyporheic exchange is the dominant mechanism for the transfer of small (sub-) pore-scale MPs into streambed sediments as was suggested before by Drummond et al. (2020, 2022).

Although the general patterns of MPs infiltration into the bedform structure were similar for all particles, there were differences in the infiltration dynamics, in particular the timing of the onset of detectable infiltration and the maximum penetration depth. Based on the arrival of the MPs plume below the ripple crest, all particles propagated rapidly into the first few centimeters of the bedform, and vertical propagation velocity decreased approximately exponentially with depth. This behavior matched the hyporheic flow field as expected from the
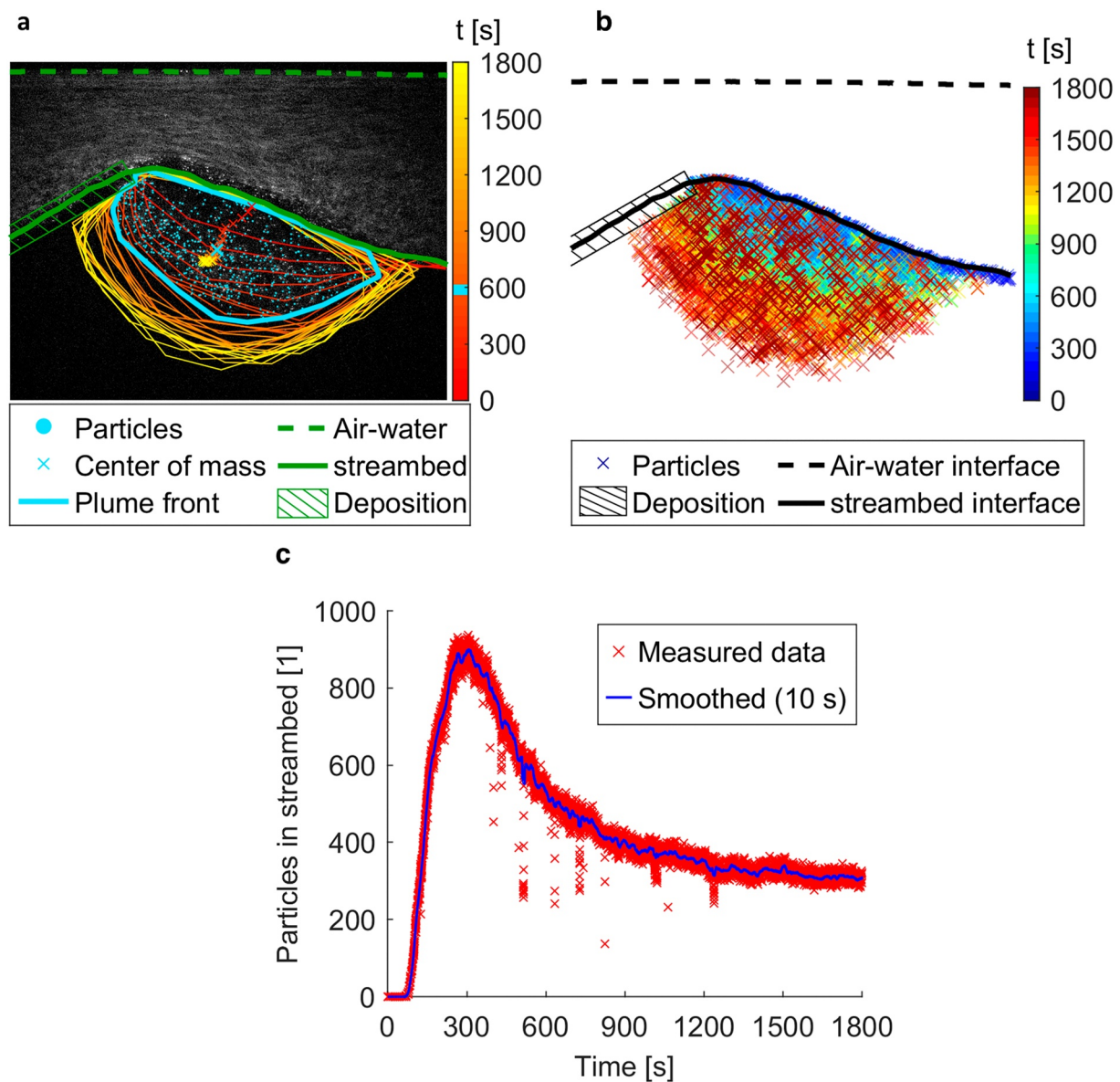
Figure 7. Infiltration experiment with 10 μm particles, analyzed by single particle tracking. (a) Particle center of mass (crosses) and plume fronts (solid lines) over time. The results are shown in 60 s-intervals during the experiment and highlighted after 600 s (cyan color), at which time also the background image was acquired, additionally indicating the detected particles (blobs). (b) Superposition of individual particle positions in the streambed, shown in 60 s-intervals during the experiment, and color-coded (blue to red), indicating the time since the start of the experiment. The air-water and streambed interfaces as well as the mask used to differentiate between infiltrated and deposited particles are shown in black. (c) Number of all particles detected in the monitored streambed section over time (red crosses), complemented by rolling mean over 10 s (blue solid line).

advective pumping model that is often used to describe bedform induced hyporheic exchange (Elliott, 1991; Grant et al., 2020; Saenger, 2000; Zhou & Mendoza, 1993). The CFD model supported this finding and additionally indicated that particle retardation in the streambed sediment increased with flow path length (Dichgans et al., 2023).

Waldschläger and Schüttrumpf (2020) used the particle/sediment grain size ratio $D = d_{MP} \, d_S^{-1}$ as a reliable indicator for the penetration depths of MPs into sediments. Column experiments showed that infiltration did not occur for $D > 0.32$ and penetration depths were highest for $D < 0.11$. Although the number of experiments performed in our study was limited, we also observed that higher particle/sediment grain size ratios tended to result in lower penetration depths and delayed onset of infiltration. For example, we observed the highest penetration depth of 11 cm for lowest $D = 0.001$ (1 μm particles) and a lower penetration depth of 7 cm for highest $D = 0.01$ (10 μm

particles). However, it is important to note that the 3 μm particles in coarse sediment (D = 0.0029) infiltrated deeper into the sediment (10 cm), than the 1 μm particles in fine sediment (D = 0.0028), where a maximum depth of 5 cm was observed. Although the particle/sediment grain size ratio has been identified as a reliable indicator for the infiltration depths of MPs into sediments, the relationship between D and penetration depths for bedform-induced hyporheic exchange may not be as straightforward as in one-dimensional column experiments where infiltration occurs vertically. While column studies indicate that mechanical straining becomes relevant for D > 0.002 (Bradford et al., 2002; Lu, Gilfedder, Peng, Niu, & Frei, 2021), the specific mechanism of particle entrainment in the streambed cannot be elucidated with the present data set. Various mechanisms influence particle transport in porous media, such as mechanical straining in the pore throats and attachment to the streambed sediments (Molnar et al., 2015). The impact of straining reduces with infiltration depth, and small particles (1–3 μm) retained deeper within the streambed may be affected more by colloid attachment (Bradford et al., 2003), which can lead to reversible as well as irreversible filtration (Chu et al., 2019). The quick decrease in concentrations of MPs and their low residuals at the end of the experiment for the 1 μm, 3 μm and high-flow experiment suggested that particle retention in the streambed was caused by reversible processes potentially facilitated by the use of deionized water in the experiment (Torkzaban et al., 2010). The retention of 10 μm particles in the streambed however suggests that mechanical straining is the dominant retention mechanism that prevents the deeper propagation of the particles into the streambed sediments.

Our experiments indicate that (sub-) pore-scale MPs exhibit high mobility in streambed sediments. In natural fluvial systems, infiltration depth is likely to exceed the depths observed in our controlled flume experiments. Bedform-driven hyporheic exchange and stream/groundwater interactions occur at various spatial and temporal scales and are influenced by multiple factors (Boano et al., 2014). Deeper hyporheic flow cells induced by head gradient variations over larger bedform structures, such as pool-riffle sequences (Frei et al., 2018), have the potential to transport particles deeper into hyporheic sediments. Also, under losing conditions where stream water infiltrates into the aquifer, mobile pore-scale MPs can be transferred into groundwater as suggested by Frei et al. (2019). In addition, hyporheic exchange is influenced by heterogeneous streambed conductivities (Laube et al., 2018; Marion et al., 2008), affecting the transport of MPs from the surface water into the streambed.

For most experiments, mass fractions of particles that entered the streambed sediments in the study domain of the flume were relatively low in comparison to particle transport in the surface water. In addition to particle size and sediment properties, particle retardation in the streambed sediments was influenced by the hydrodynamic forcing. This controls the magnitudes of advective flow velocities and volumes in the streambed sediments during hyporheic exchange. An increase in the surface flow velocity (high flow experiment) resulted in the fastest observed MPs breakthrough, and almost no residual particles were detected in the bedform at the end of the experiment, unlike in the low flow experiments. Flooding events have been recognized as significant drivers of MPs remobilization from streambed sediments, with reductions in MPs loads stored in sediments of up to 70% as reported by Hurley et al. (2018). During flooding, shear forces acting at the streambed interface lead to erosion of the bedform structures. This results in the suspension of river sediments and associated MPs and its transport through the river network. Results from our study suggest that in addition to flooding events, streambed sediments may be effectively flushed of pore-scale MPs during periods of increased discharge, under conditions when bedform structures remain stable.

In the fine sediment experiment, mass balance calculations based on the surface breakthrough curves indicated that a significant fraction of the inflowing particles (22%) was present in the study domain at the end of the experiment. Although particles can be retained in surface flow, for example, due to entrapment in recirculation eddies and at the streambed interface due to heteroaggregation, this effect was not observed in the other experiments given similar hydrodynamic conditions. This suggests that surface retention was of minor importance in the flume experiments and that most particles were retarded in the streambed sediments. This conclusion is supported by the FIS monitoring, which did not detect any trend in increasing particle concentrations in the areas where eddies are present or at the streambed interface.

Based on our experiments, we have found that fine sediment areas in streambeds have the potential to accumulate (sub-) pore-scale MPs where mechanical straining reduces particle mobility. While the duration of our flume experiments was insufficient to determine whether the particles were immobilized permanently or temporarily, results from particle tracking of 10 μm MPs suggest that a considerable portion of infiltrated particles showed a prolonged residence time. Pore-scale MPs that become immobile in fine sediment areas of streambeds pose an

increased risk for uptake by benthic organisms, since longer exposure times increase the likelihood of ingestion. Under these conditions, hyporheic sediments are especially vulnerable to MPs accumulation and can represent a primary entry point for MPs into riverine food webs (Huang et al., 2021; Wagner et al., 2014). Fine sediment loadings in many rivers and streams have been observed to exceed background levels, primarily due to changes in land cover, land use, and management practices (Collins & Zhang, 2016; Farnsworth & Milliman, 2003; Foster et al., 2011; Owens et al., 2005). It is anticipated that the trend of increasing fine sediment loadings in rivers and streams will persist in the future, due to the effects of climate change on rainfall and runoff regimes (Burt et al., 2016; Walling & Collins, 2016). This may also lead to a further accumulation of MPs in streambed sediments, exacerbating the existing issue.

This study analyzed the transport of almost neutrally buoyant MPs. Density is a key factor controlling particle transport, which can be transported floating, suspended or as bedload (Waldschläger et al., 2022). For larger particles between 1–3 mm, the location of MPs in the water column is similar to mineral sediments (Born et al., 2023), indicating that higher density MPs are more likely to be transported near the streambed. Conversely, turbulent mixing, such as caused by the weir overflow in our experiment, can also transport low density MPs to the streambed interface (Shamskhany & Karimpour, 2022). Within streambed sediments, low-density MPs, such as polyethylene and polypropylene, exhibit higher mobility, whereas high-density MPs, auch as polyamide and polyethylene terephthalate, are retained (He et al., 2021). The hydrodynamic behavior is influenced by additional processes under real environmental conditions. Biofilms on the surface of MPs facilitate the formation of heteroaggregates, as particles become "sticky" due to attached extracellular polymeric substances (Hossain et al., 2019; Long et al., 2015; Michels et al., 2018). While the formation of biofilms is typically more prevalent in lentic systems, it has been reported to be relevant in rivers and streams (Weig et al., 2021). Biofilms may form on MPs prior to entering fluvial systems, for example, due to their passage through wastewater treatment plants or in soils (Martínez-Campos et al., 2021; Zhang et al., 2019). The adhesive properties of biofilms may enhance the likelihood of particle heteroaggregation on the streambed, rather than being transported into the sediment via hyporheic exchange. Also, larger heteroaggregates containing both MPs and natural particles are not able to infiltrate into the streambed sediments as readily as individual, pristine particles.

Our experiments focused on the infiltration of microplastics into a stationary rippled streambed. Under natural conditions, bedform structures are rarely stable long-term. Small-scale hydrodynamical conditions create highly dynamic areas of erosion and sedimentation. As a result, bedform structures such as ripples or dunes migrate as "moving bedforms" in the direction of streamflow (Southard, 1991). The exchange of solutes and colloids between surface flow and streambed can be significantly higher for moving bedforms compared to stable bedform structures (Packman & Brooks, 2001). Recent flume experiments have demonstrated that dynamic sedimentation and erosion processes result in the preferential accumulation of clay particles within streambed sediments (Teitelbaum et al., 2021). Future research must address whether the accumulation of MPs within moving bedforms occurs similarly to that of clay particles and whether the erosion and sedimentation cycles associated with moving bedforms enhance the transfer of MPs into streambed sediments, as compared to stable bedforms where MPs exchange is purely driven by bedform-induced hyporheic exchange.

5. Conclusion

In analogy to solute transport, advective transport has been suggested as one potential mechanism driving the exchange of (sub-) pore-scale MPs between surface water and the streambed. This study confirms this hypothesis, as we were able to detect MPs migration between surface flow and streambed sediments and additionally link particle transport to the hydrodynamic characteristics of the flow. Smaller particles (1–3 µm) showed higher mobility and infiltrated into deeper areas of the sediment, while larger particles (10 µm) were retained in shallower parts of the streambed. Streambed sediment grain size had a major influence on the pattern of particle infiltration and retardation in the streambed.

Our results suggest that MPs are concentrated in the upper sediment layers in natural streams and show enhanced residence times within finer sediments. A prolonged immobilization near the streambed interface enhances the potential of particle uptake by benthic organisms and subsequent transfer within the aquatic food chain, possibly threatening local ecosystems. More work is needed to transfer the mechanistic understanding of MPs transport processes from laboratory experiments to real-world scenarios in order to improve our understanding of the fate of MPs in rivers and streams.

Conflict of Interest

The authors declare no conflicts of interest relevant to this study.

Data Availability Statement

The data sets as well as the developed MATLAB scripts are published in Zenodo (Boos et al., 2023a; 2023b).

References

Ahmadi, P., Elagami, H., Dichgans, F., Schmidt, C., Gilfedder, B. S., Frei, S., et al. (2022). Systematic evaluation of physical parameters affecting the terminal settling velocity of microplastic particles in lakes using CFD. *Frontiers in Environmental Science*, *10*. https://doi.org/10.3389/fenvs.2022.875220

Anbumani, S., & Kakkar, P. (2018). Ecotoxicological effects of microplastics on biota: A review. *Environmental Science and Pollution Research International*, *25*(15), 14373–14396. https://doi.org/10.1007/s11356-018-1999-x

Bhatt, V., & Chauhan, J. S. (2023). Microplastic in freshwater ecosystem: Bioaccumulation, trophic transfer, and biomagnification. *Environmental Science and Pollution Research International*, *30*(4), 9389–9400. https://doi.org/10.1007/s11356-022-24529-w

Boano, F., Harvey, J. W., Marion, A., Packman, A. I., Revelli, R., Ridolfi, L., & Wörman, A. (2014). Hyporheic flow and transport processes: Mechanisms, models, and biogeochemical implications. *Reviews of Geophysics*, *52*(4), 603–679. https://doi.org/10.1002/2012RG000417

Boos, J.-P., Dichgans, F., Fleckenstein, J. H., Gilfedder, B. S., & Frei, S. (2023). Data and code for the publication "Assessing the behavior of microplastics in fluvial systems: Infiltration and retention dynamics in streambed sediments" - Part 1. https://doi.org/10.5281/zenodo.10083568

Boos, J.-P., Dichgans, F., Fleckenstein, J. H., Gilfedder, B. S., & Frei, S. (2023). Data and code for the publication "Assessing the behavior of microplastics in fluvial systems: Infiltration and retention dynamics in streambed sediments" - Part 2. https://doi.org/10.5281/zenodo.10081788

Boos, J.-P., Gilfedder, B. S., & Frei, S. (2021). Tracking microplastics across the streambed interface: Using laser-induced-fluorescence to quantitatively analyze microplastic transport in an experimental flume. *Water Resources Research*, *57*(12). https://doi.org/10.1029/2021WR031064

Born, M. P., Brüll, C., Schaefer, D., Hillebrand, G., & Schüttrumpf, H. (2023). Determination of microplastics' vertical concentration transport (Rouse) profiles in flumes. *Environmental Science & Technology*, *57*(14), 5569–5579. https://doi.org/10.1021/acs.est.2c06885

Bradford, S. A., Simunek, J., Bettahar, M., van Genuchten, M. T., & Yates, S. R. (2003). Modeling colloid attachment, straining, and exclusion in saturated porous media. *Environmental Science & Technology*, *37*(10), 2242–2250. https://doi.org/10.1021/es025899u

Bradford, S. A., Yates, S. R., Bettahar, M., & Simunek, J. (2002). Physical factors affecting the transport and fate of colloids in saturated porous media. *Water Resources Research*, *38*(12), 63-1–63-12. https://doi.org/10.1029/2002WR001340

Brehm, J., Wilde, M. V., Reiche, L., Leitner, L.-C., Petran, B., Meinhart, M., et al. (2022). In-depth characterization revealed polymer type and chemical content specific effects of microplastic on Dreissena bugensis. *Journal of Hazardous Materials*, *437*, 129351. https://doi.org/10.1016/j.jhazmat.2022.129351

Brunke, M. (1999). Colmation and depth filtration within streambeds: Retention of particles in hyporheic interstices. *International Review of Hydrobiology*, *84*(2), 99–117. https://doi.org/10.1002/iroh.199900014

Burt, T., Boardman, J., Foster, I., & Howden, N. (2016). More rain, less soil: Long-term changes in rainfall intensity with climate change. *Earth Surface Processes and Landforms*, *41*(4), 563–566. https://doi.org/10.1002/esp.3868

Chu, X., Li, T., Li, Z., Yan, A., & Shen, C. (2019). Transport of microplastic particles in saturated porous media. *Water*, *11*(12), 2474. https://doi.org/10.3390/w11122474

Collins, A. L., & Zhang, Y. (2016). Exceedance of modern 'background' fine-grained sediment delivery to rivers due to current agricultural land use and uptake of water pollution mitigation options across England and Wales. *Environmental Science & Policy*, *61*, 61–73. https://doi.org/10.1016/j.envsci.2016.03.017

Dichgans, F., Boos, J.-P., Ahmadi, P., Frei, S., & Fleckenstein, J. H. (2023). Integrated numerical modeling to quantify transport and fate of microplastics in the hyporheic zone. *Water Research*, *243*, 120349. https://doi.org/10.1016/j.watres.2023.120349

Drummond, J. D., Nel, H. A., Packman, A. I., & Krause, S. (2020). Significance of hyporheic exchange for predicting microplastic fate in rivers. *Environmental Science and Technology Letters*, *7*(10), 727–732. https://doi.org/10.1021/acs.estlett.0c00595

Drummond, J. D., Schneidewind, U., Li, A., Hoellein, T. J., Krause, S., & Packman, A. I. (2022). Microplastic accumulation in riverbed sediment via hyporheic exchange from headwaters to mainstems. *Science Advances*, *8*(2), eabi9305. https://doi.org/10.1126/sciadv.abi9305

Eerkes-Medrano, D., Thompson, R. C., & Aldridge, D. C. (2015). Microplastics in freshwater systems: A review of the emerging threats, identification of knowledge gaps and prioritisation of research needs. *Water Research*, *75*, 63–82. https://doi.org/10.1016/j.watres.2015.02.012

Eibes, P. M., & Gabel, F. (2022). Floating microplastic debris in a rural river in Germany: Distribution, types and potential sources and sinks. *The Science of the Total Environment*, *816*, 151641. https://doi.org/10.1016/j.scitotenv.2021.151641

Elagami, H., Ahmadi, P., Fleckenstein, J. H., Frei, S., Obst, M., Agarwal, S., & Gilfedder, B. S. (2022). Measurement of microplastic settling velocities and implications for residence times in thermally stratified lakes. *Limnology & Oceanography*, *67*(4), 934–945. https://doi.org/10.1002/lno.12046

Elliott, A. H. (1991). *Transfer of solutes into and out of streambeds*. California Institute of Technology.

Elliott, A. H., & Brooks, N. H. (1997). Transfer of nonsorbing solutes to a streambed with bed forms: Laboratory experiments. *Water Resources Research*, *33*(1), 137–151. https://doi.org/10.1029/96WR02783

Farnsworth, K. L., & Milliman, J. D. (2003). Effects of climatic and anthropogenic change on small mountainous rivers: The Salinas river example. *Global and Planetary Change*, *39*(1–2), 53–64. https://doi.org/10.1016/S0921-8181(03)00017-1

Foster, I., Collins, A. L., Naden, P. S., Sear, D. A., Jones, J. I., & Zhang, Y. (2011). The potential for paleolimnology to determine historic sediment delivery to rivers. *Journal of Paleolimnology*, *45*(2), 287–306. https://doi.org/10.1007/s10933-011-9498-9

Frei, S., Azizian, M., Grant, S. B., Zlotnik, V. A., & Toundykov, D. (2018). Analytical modeling of hyporheic flow for in-stream bedforms: Perturbation method and implementation. *Environmental Modelling & Software*. (111), 375–385. https://doi.org/10.1016/j.envsoft.2018.09.015

Frei, S., Piehl, S., Gilfedder, B. S., Löder, M. G. J., Krutzke, J., Wilhelm, L., & Laforsch, C. (2019). Occurrence of microplastics in the hyporheic zone of rivers. *Scientific Reports*, *9*(1), 15256. https://doi.org/10.1038/s41598-019-51741-1

Frias, J. P. G. L., & Nash, R. (2019). Microplastics: Finding a consensus on the definition. *Marine Pollution Bulletin*, *138*, 145–147. https://doi.org/10.1016/j.marpolbul.2018.11.022

Funk, W., Dammann, V., Vonderheid, C., & Oehlmann, G. (Eds.) (1985). *Statistische Methoden in der Wasseranalytik: Begriffe, Strategien, Anwendungen*. VCH.

Gola, D., Kumar Tyagi, P., Arya, A., Chauhan, N., Agarwal, M., Singh, S. K., & Gola, S. (2021). The impact of microplastics on marine environment: A review. *Environmental Nanotechnology, Monitoring & Management*, *16*, 100552. https://doi.org/10.1016/j.enmm.2021.100552

Grant, S. B., Monofy, A., Boano, F., Gomez-Velez, J. D., Guymer, I., Harvey, J. W., & Ghisalberti, M. (2020). Unifying advective and diffusive descriptions of bedform pumping in the benthic biolayer of streams. *Water Resources Research*, *56*(11). https://doi.org/10.1029/2020WR027967

Haberstroh, C. J., Arias, M. E., Yin, Z., & Wang, M. C. (2020). Effects of hydrodynamics on the cross-sectional distribution and transport of plastic in an urban coastal river. *Water Environment Research*, *93*(2), 186–200. https://doi.org/10.1002/wer.1386

Haque, M. I., & Mahmood, K. (1985). Geometry of ripples and dunes. *Journal of Hydraulic Engineering*, *111*(1), 48–63. https://doi.org/10.1061/(ASCE)0733-9429(1985)111:1(48)

Harvey, J. W., Drummond, J. D., Martin, R. L., McPhillips, L. E., Packman, A. I., Jerolmack, D. J., et al. (2012). Hydrogeomorphology of the hyporheic zone: Stream solute and fine particle interactions with a dynamic streambed. *Journal of Geophysical Research*, *117*(G4). https://doi.org/10.1029/2012JG002043

He, B., Smith, M., Egodawatta, P., Ayoko, G. A., Rintoul, L., & Goonetilleke, A. (2021). Dispersal and transport of microplastics in river sediments. *Environmental Pollution*, *279*, 116884. https://doi.org/10.1016/j.envpol.2021.116884

Herzig, J. P., Leclerc, D. M., & Goff, P. L. (1970). Flow of suspensions through porous media—Application to deep filtration. *Industrial & Engineering Chemistry*, *62*(5), 8–35. https://doi.org/10.1021/ie50725a003

Horton, A. A., & Dixon, S. J. (2018). Microplastics: An introduction to environmental transport processes. *Wiley Interdisciplinary Reviews: Water*, *5*(2), e1268. https://doi.org/10.1002/wat2.1268

Hossain, M. R., Jiang, M., Wei, Q., & Leff, L. G. (2019). Microplastic surface properties affect bacterial colonization in freshwater. *Journal of Basic Microbiology*, *59*(1), 54–61. https://doi.org/10.1002/jobm.201800174

Huang, W., Song, B., Liang, J., Niu, Q., Zeng, G., Shen, M., et al. (2021). Microplastics and associated contaminants in the aquatic environment: A review on their ecotoxicological effects, trophic transfer, and potential impacts to human health. *Journal of Hazardous Materials*, *405*, 124187. https://doi.org/10.1016/j.jhazmat.2020.124187

Hübner, M. K., Michler-Kozma, D. N., & Gabel, F. (2020). Microplastic concentrations at the water surface are reduced by decreasing flow velocities caused by a reservoir. *Fundamental and Applied Limnology*, *194*(1), 49–56. https://doi.org/10.1127/fal/2020/1307

Hurley, R., Woodward, J., & Rothwell, J. J. (2018). Microplastic contamination of river beds significantly reduced by catchment-wide flooding. *Nature Geoscience*, *11*(4), 251–257. https://doi.org/10.1038/s41561-018-0080-1

Janssen, F., Cardenas, M. B., Sawyer, A. H., Dammrich, T., Krietsch, J., & de. Beer, D. (2012). A comparative experimental and multiphysics computational fluid dynamics study of coupled surface-subsurface flow in bed forms. *Water Resources Research*, *48*(8). https://doi.org/10.1029/2012WR011982

Kumar, R., Sharma, P., Manna, C., & Jain, M. (2021). Abundance, interaction, ingestion, ecological concerns, and mitigation policies of microplastic pollution in riverine ecosystem: A review. *Science of the Total Environment*, *782*, 146695. https://doi.org/10.1016/j.scitotenv.2021.146695

Kumar, R., Sharma, P., Verma, A., Jha, P. K., Singh, P., Gupta, P. K., et al. (2021). Effect of physical characteristics and hydrodynamic conditions on transport and deposition of microplastics in riverine ecosystem. *Water*, *13*(19), 2710. https://doi.org/10.3390/w13192710

Laube, G., Schmidt, C., & Fleckenstein, J. H. (2018). The systematic effect of streambed conductivity heterogeneity on hyporheic flux and residence time. *Advances in Water Resources*, *122*, 60–69. https://doi.org/10.1016/j.advwatres.2018.10.003

Lebreton, L., & Andrady, A. (2019). Future scenarios of global plastic waste generation and disposal. *Palgrave Communications*, *5*(1), 6. https://doi.org/10.1057/s41599-018-0212-7

Liong, R. M. Y., Hadibarata, T., Yuniarto, A., Tang, K. H. D., & Khamidun, M. H. (2021). Microplastic occurrence in the water and sediment of Miri river estuary, Borneo island. *Water, Air, & Soil Pollution*, *232*(8), 342. https://doi.org/10.1007/s11270-021-05297-8

Long, M., Moriceau, B., Gallinari, M., Lambert, C., Huvet, A., Raffray, J., & Soudant, P. (2015). Interactions between microplastics and phytoplankton aggregates: Impact on their respective fates. *Marine Chemistry*, *175*, 39–46. https://doi.org/10.1016/j.marchem.2015.04.003

Lu, T., Gilfedder, B. S., Peng, H., Niu, G., & Frei, S. (2021). Effects of clay minerals on the transport of nanoplastics through water-saturated porous media. *The Science of the Total Environment*, *796*, 148982. https://doi.org/10.1016/j.scitotenv.2021.148982

Lu, T., Gilfedder, B. S., Peng, H., Peiffer, S., Papastavrou, G., Ottermann, K., & Frei, S. (2021). Relevance of iron oxyhydroxide and pore water chemistry on the mobility of nanoplastic particles in water-saturated porous media environments. *Water, Air, & Soil Pollution*, *232*(5), 168. https://doi.org/10.1007/s11270-021-05125-z

Marion, A., Packman, A. I., Zaramella, M., & Bottacin-Busolin, A. (2008). Hyporheic flows in stratified beds. *Water Resources Research*, *44*(9). https://doi.org/10.1029/2007WR006079

Martínez-Campos, S., González-Pleiter, M., Fernández-Piñas, F., Rosal, R., & Leganés, F. (2021). Early and differential bacterial colonization on microplastics deployed into the effluents of wastewater treatment plants. *The Science of the Total Environment*, *757*, 143832. https://doi.org/10.1016/j.scitotenv.2020.143832

Meijer, L. J. J., van Emmerik, T., van der Ent, R., Schmidt, C., & Lebreton, L. (2021). More than 1000 rivers account for 80% of global riverine plastic emissions into the ocean. *Science Advances*, *7*(18). https://doi.org/10.1126/sciadv.aaz5803

Michels, J., Stippkugel, A., Lenz, M., Wirtz, K., & Engel, A. (2018). Rapid aggregation of biofilm-covered microplastics with marine biogenic particles. *Proceedings of the Royal Society: Biological Sciences*, *285*(1885), 20181203. https://doi.org/10.1098/rspb.2018.1203

Molnar, I. L., Johnson, W. P., Gerhard, J. I., Willson, C. S., & O'Carroll, D. M. (2015). Predicting colloid transport through saturated porous media: A critical review. *Water Resources Research*, *51*(9), 6804–6845. https://doi.org/10.1002/2015WR017318

Mostefaoui, O., Lopez, D., Mignot, E., & Massardier-Nageotte, V. (2022). Extended Abstract CFTL 2022.

Ockelford, A., Cundy, A., & Ebdon, J. E. (2020). Storm response of fluvial sedimentary microplastics. *Scientific Reports*, *10*(1), 1865. https://doi.org/10.1038/s41598-020-58765-2

Owens, P. N., Batalla, R. J., Collins, A. J., Gomez, B., Hicks, D. M., Horowitz, A. J., et al. (2005). Fine-grained sediment in river systems: Environmental significance and management issues. *River Research and Applications*, *21*(7), 693–717. https://doi.org/10.1002/rra.878

Packman, A. I., & Brooks, N. H. (2001). Hyporheic exchange of solutes and colloids with moving bed forms. *Water Resources Research*, *37*(10), 2591–2605. https://doi.org/10.1029/2001WR000477

Persson, L., Carney Almroth, B. M., Collins, C. D., Cornell, S., de Wit, C. A., Diamond, M. L., et al. (2022). Outside the safe operating space of the planetary boundary for novel entities. *Environmental Science & Technology*, *56*(3), 1510–1521. https://doi.org/10.1021/acs.est.1c04158

PlasticsEurope. (2022). Plastics—The facts 2022.

Rolf, M., Laermanns, H., Kienzler, L., Pohl, C., Möller, J. N., Laforsch, C., et al. (2022). Flooding frequency and floodplain topography determine abundance of microplastics in an alluvial Rhine soil. *The Science of the Total Environment*, *836*, 155141. https://doi.org/10.1016/j.scitotenv.2022.155141

Saenger, N. (2000). *Identifikation von Austauschprozessen zwischen Fließgewässer und hyporheischer Zone* (Vol. 115). Technische Universität Darmstadt.

Scherer, C., Weber, A., Lambert, S., & Wagner, M. (2018). Interactions of microplastics with freshwater biota. In M. Wagner & S. Lambert (Eds.), *The handbook of environmental chemistry, Freshwater microplastics* (Vol. 58, pp. 153–180). Springer International Publishing. https://doi.org/10.1007/978-3-319-61615-5_8

Shamskhany, A., & Karimpour, S. (2022). Entrainment and vertical mixing of aquatic microplastics in turbulent flow: The coupled role of particle size and density. *Marine Pollution Bulletin*, *184*, 114160. https://doi.org/10.1016/j.marpolbul.2022.114160

Shi, W., Peruzzo, P., & Defina, A. (2022). Transient retention of floating particles captured by emergent vegetation through capillarity. *Water Resources Research*, *58*(6). https://doi.org/10.1029/2022WR031964

Southard, J. B. (1991). Experimental determination of bed-form stability. *Annual Review of Earth and Planetary Sciences*, *19*(1), 423–455. https://doi.org/10.1146/annurev.ea.19.050191.002231

Teitelbaum, Y., Dallmann, J., Phillips, C. B., Packman, A. I., Schumer, R., Sund, N. L., et al. (2021). Dynamics of hyporheic exchange flux and fine particle deposition under moving bedforms. *Water Resources Research*, *57*(4). https://doi.org/10.1029/2020WR028541

The MathWorks Inc. (2019). MATLAB and image processing toolbox R2019b.

Thibodeaux, L. J., & Boyle, J. D. (1987). Bedform-generated convective transport in bottom sediment. *Nature*, *325*(6102), 341–343. https://doi.org/10.1038/325341a0

Torkzaban, S., Kim, H. N., Simunek, J., & Bradford, S. A. (2010). Hysteresis of colloid retention and release in saturated porous media during transients in solution chemistry. *Environmental Science & Technology*, *44*(5), 1662–1669. https://doi.org/10.1021/es903277p

Trauth, N., Schmidt, C., Vieweg, M., Maier, U., & Fleckenstein, J. H. (2014). Hyporheic transport and biogeochemical reactions in pool-riffle systems under varying ambient groundwater flow conditions. *Journal of Geophysical Research: Biogeosciences*, *119*(5), 910–928. https://doi.org/10.1002/2013JG002586

Valero, D., Belay, B. S., Moreno-Rodenas, A., Kramer, M., & Franca, M. J. (2022). The key role of surface tension in the transport and quantification of plastic pollution in rivers. *Water Research*, *226*, 119078. https://doi.org/10.1016/j.watres.2022.119078

Van Emmerik, T., Mellink, Y., Hauk, R., Waldschläger, K., & Schreyers, L. (2022). Rivers as plastic reservoirs. *Frontiers in Water*, *3*. https://doi.org/10.3389/frwa.2021.786936

Wagner, M., Scherer, C., Alvarez-Muñoz, D., Brennholt, N., Bourrain, X., Buchinger, S., et al. (2014). Microplastics in freshwater ecosystems: What we know and what we need to know. *Environmental Sciences Europe*, *26*(1), 12. https://doi.org/10.1186/s12302-014-0012-7

Waldschläger, K., Brückner, M. Z., Carney Almroth, B., Hackney, C. R., Adyel, T. M., Alimi, O. S., et al. (2022). Learning from natural sediments to tackle microplastics challenges: A multidisciplinary perspective. *Earth-Science Reviews*, *228*, 104021. https://doi.org/10.1016/j.earscirev.2022.104021

Waldschläger, K., & Schüttrumpf, H. (2019). Erosion behavior of different microplastic particles in comparison to natural sediments. *Environmental Science & Technology*, *53*(22), 13219–13227. https://doi.org/10.1021/acs.est.9b05394

Waldschläger, K., & Schüttrumpf, H. (2020). Infiltration behavior of microplastic particles with different densities, sizes, and shapes-from glass spheres to natural sediments. *Environmental Science & Technology*, *54*(15), 9366–9373. https://doi.org/10.1021/acs.est.0c01722

Walling, D. E., & Collins, A. L. (2016). Fine sediment transport and management. In D. J. Gilvear, M. T. Greenwood, M. C. Thoms, & P. J. Wood (Eds.), *River science* (pp. 37–60). John Wiley & Sons, Ltd. https://doi.org/10.1002/9781118643525.ch3

Weig, A. R., Löder, M. G. J., Ramsperger, A. F. R. M., & Laforsch, C. (2021). In situ prokaryotic and eukaryotic communities on microplastic particles in a small headwater stream in Germany. *Frontiers in Microbiology*, *12*, 660024. https://doi.org/10.3389/fmicb.2021.660024

Woodall, L. C., Sanchez-Vidal, A., Canals, M., Paterson, G. L. J., Coppock, R., Sleight, V., et al. (2014). The deep sea is a major sink for microplastic debris. *Royal Society Open Science*, *1*(4), 140317. https://doi.org/10.1098/rsos.140317

Yang, L., Zhang, Y., Kang, S., Wang, Z., & Wu, C. (2021). Microplastics in freshwater sediment: A review on methods, occurrence, and sources. *The Science of the Total Environment*, *754*, 141948. https://doi.org/10.1016/j.scitotenv.2020.141948

Yang, S., Zhou, M., Chen, X., Hu, L., Xu, Y., Fu, W., & Li, C. (2022). A comparative review of microplastics in lake systems from different countries and regions. *Chemosphere*, *286*(2), 131806. https://doi.org/10.1016/j.chemosphere.2021.131806

Zhang, M., Zhao, Y., Qin, X., Jia, W., Chai, L., Huang, M., & Huang, Y. (2019). Microplastics from mulching film is a distinct habitat for bacteria in farmland soil. *The Science of the Total Environment*, *688*, 470–478. https://doi.org/10.1016/j.scitotenv.2019.06.108

Zhou, D., & Mendoza, C. (1993). Flow through porous bed of turbulent stream. *Journal of Engineering Mechanics*, *119*(2), 365–383. https://doi.org/10.1061/(ASCE)0733-9399(1993)119:2(365)